Exciton interference in hexagonal boron nitride

Lorenzo Sponza, Hakim Amara, François Ducastelle, and Annick Loiseau
LEM UMR 104, ONERA–CNRS, F-92322 Châtillon, France

Claudio Attaccalite
CINaM UMR 7325, Aix-Marseille University–CNRS, F-13288 Marseille, France

In this letter we report a thorough analysis of the exciton dispersion in bulk hexagonal boron nitride. We solve the *ab initio* GW Bethe-Salpeter equation at finite $\mathbf{q} \parallel \Gamma K$, which is relevant for spectroscopic measurements. Simulations reproduce the dispersion and the intensity of recent high-accuracy electron energy loss data. We demonstrate that the excitonic peak comes from the interference of two groups of transitions involving the points K and K' of the Brillouin zone. The number and the amplitude of these transitions determine variations in the peak intensity. Our results contribute to the understanding of electronic excitations in this system, unveiling a nontrivial relation between valley physics and excitonic properties. Furthermore, the methodology introduced in this study to regroup independent-particle transitions is completely general and can be applied successfully to the investigation of excitonic properties in any system.

I. INTRODUCTION

Hexagonal boron nitride (*h*–BN) is a layered crystal homostructural to graphite. It displays peculiar optoelectronic properties, measured notably with luminescence [1–4], x rays [5,6], or angular resolved electron energy loss spectroscopy (EELS) [7,8]. Several studies have been carried out on its excitonic properties, however, some fundamental aspects are still controversial. For instance, established theoretical calculations predict *h*–BN to be an indirect gap insulator [6,9], and this seems to be confirmed by recent photoluminescence data [3], but this conclusion contrasts with the experimental finding of strong luminescence in *h*–BN crystals [1], not compatible with a phonon-assisted excitation picture. In this context high-accuracy EELS measurements have been performed very recently [7] at momenta $0.1\,\text{Å}^{-1} \leqslant \mathbf{q} \leqslant 1.1\,\text{Å}^{-1}$ parallel to the ΓK direction of the first Brillouin zone. The authors give an account of an excitonic peak dispersing approximately 0.2 eV, reaching the highest intensity and minimum excitation energy at about $0.7\,\text{Å}^{-1}$ and almost disappearing at $1.1\,\text{Å}^{-1}$.

Finite-momentum EELS give access to the energy- and momentum-dependent loss function,

$$L(\mathbf{q},\omega) = \text{Im}[\epsilon(\mathbf{q},\omega)]/|\epsilon(\mathbf{q},\omega)|^2, \qquad (1)$$

which gives information about the dielectric function $\epsilon(\mathbf{q},\omega)$ of the probed material. Peaks of $L(\mathbf{q},\omega)$ can be put in relation with interband excitations $\{\propto \text{Im}[\epsilon(\mathbf{q},\omega)]\}$ and plasmon resonances ($|\epsilon| \approx 0$). So far, measures have been reproduced, interpreted and even anticipated by *ab initio* simulations based on the Bethe-Salpeter equation (BSE) formalism [10], which includes explicitly the electron-hole interaction (the exciton). A very general behavior, observed in the recent EELS measures [7] as well, is a sizable variation of the intensity of $L(\mathbf{q},\omega)$ as a function of the exchanged momentum $\mathbf{q}$, notably the

enhancement or the attenuation of excitonic peaks along their dispersion [6,11,12].

In this article we devise accurate numerical methods based on the BSE for the analysis of excitonic features. We applied them to the investigation of the loss function of bulk *h*–BN in the same energy and momentum conditions as in [7], confirming the excitonic nature of the peak, clarifying the origin of its enhancement at $0.7\,\text{Å}^{-1}$ and its dramatic attenuation at higher momentum. Our analysis provides a deep insight into the electronic excitations of *h*–BN and it unveils a nontrivial valley physics, indicating possible ways to tune the exciton intensity. More importantly, the approach introduced here is of general applicability. We believe that this approach constitutes a helpful way to understand and control excitonic properties in any system. We are convinced that the outcome of our analysis provides the key ingredients to explain similar effects observed in other materials [6,11,12]. Furthermore, it provides a general methodology to identify how and where the electronic structure has to be modified to achieve the desired exciton intensity.

II. NUMERICAL ANALYSIS METHODS

EELS and nonresonant inelastic x-ray scattering give access to the loss function $L(\mathbf{q},\omega)$ with complementary degrees of accuracy in the $\mathbf{q}$ range [8].

Theory-wise, $L(\mathbf{q},\omega)$ can be calculated accurately from the dielectric function $\epsilon(\mathbf{q},\omega)$, obtained as a solution of the BSE. This can be cast in the form of an eigenvalue problem whose Hamiltonian is most often written in a basis of independent-particle (IP) transitions of index $t = (v,\mathbf{k}) \rightarrow (c,\mathbf{k} + \mathbf{q})$ between occupied and empty states of an underlying IP model, e.g., the Kohn-Sham system. Here $(v,\mathbf{k})$ indicate the initial state and $(c,\mathbf{k} + \mathbf{q})$ the final state, where $\mathbf{q}$ is the exchanged momentum laying inside the first Brillouin zone. Within this

framework and including only resonant transitions,

$$\epsilon(\mathbf{q},\omega) \propto \sum_\lambda \frac{I_\lambda(\mathbf{q})}{E_\lambda(\mathbf{q}) - \omega + i\eta}, \qquad (2)$$

where $E_\lambda(\mathbf{q})$ is the energy of the λth exciton [13] and η a positive infinitesimal quantity. The spectral intensity,

$$I_\lambda(\mathbf{q}) = \left| \sum_t \tilde{\rho}_t(\mathbf{q}) A_t^\lambda(\mathbf{q}) \right|^2 = \left| \sum_t M_t^\lambda(\mathbf{q}) \right|^2, \qquad (3)$$

is the modulus squared of a linear combination of IP-transition matrix elements $\tilde{\rho}_t(\mathbf{q}) = \langle v\mathbf{k}|e^{-i\mathbf{q}\cdot\mathbf{r}}|c\mathbf{k} + \mathbf{q}\rangle$ weighted by the exciton wave-function components $A_t^\lambda(\mathbf{q})$. The exciton λ is called "bright" when $I_\lambda(\mathbf{q})$ is sizeably high, and conversely it is called "dark" when $I_\lambda(\mathbf{q}) \approx 0$. This can happen if either $\tilde{\rho}_t(\mathbf{q})$ or $A_t^\lambda(\mathbf{q})$ or both are negligible for all t, or when IP transitions interfere destructively leading to a vanishing sum in expression (3). Thus it is sensible to introduce the normalized cumulant weight [11,14]:

$$\mathcal{J}_\lambda(\mathbf{q}, E) = \frac{1}{I_\lambda(\mathbf{q})} \left| \sum_{t:E_t \leqslant E} M_t^\lambda(\mathbf{q}) \right|^2, \qquad (4)$$

which allows for a visualization of the building up of the exciton spectral weight as a function of the IP-transition energy E. This function is positively defined, it tends asymptotically to 1 and in general is not monotonic.

The normalized cumulant weight (4) gives a piece of information relying on the energy of the IP transitions, although more detailed analysis can be achieved by a careful study of the single $M_t^\lambda(\mathbf{q})$ amplitudes themselves. In particular one can use the phase of $M_t^\lambda(\mathbf{q})$ to split IP transitions into groups depending on their sign in the sum (3). This allows for a deconvolution of the exciton (which includes all IP transitions) into competing groups of IP transitions, the intensity of the total peak resulting from the interplay of these contributions.

III. RESULTS

In Fig. 1 we report the simulated loss function for exchanged momenta $\mathbf{q} \parallel \Gamma K$ at intervals of $\mathbf{q}_0 = K/12 \approx 0.14 \,\text{Å}^{-1}$ (see Appendix A for computational details). In the inset, circles depict the calculated dispersion of the peak compared to the experimental data (red bullets) extracted from [7]. Beside a blue-shift of about 0.47 eV that comes from a well-known underestimation of the gap in this material within the G_0W_0 approximation [15], the calculated spectra and their dispersion are in very good agreement with the measurements. In particular our simulations reproduce the fact that the lowest-energy excitation is at $\mathbf{q} = 5\mathbf{q}_0 \approx 0.7 \,\text{Å}^{-1}$, where the peak attains its highest intensity, and that approximately at $\mathbf{q} = 8\mathbf{q}_0 \approx 1.1 \,\text{Å}^{-1}$ the peak is strongly suppressed (cf. Fig. 1 in [7]). At higher $\mathbf{q}$, the loss function increases again with abrupt intensity, reproducing the strong exciton expected at $\mathbf{q} = K$ and already analyzed elsewhere in the literature [5,6,8].

In this energy range, it turns out that $|\epsilon(\mathbf{q},\omega)|$ does not vanish; consequently Eq. (1) allows us to attribute an interband character to the excitation and establish a close relation between structures of the loss function and peaks of Im[ϵ]. This

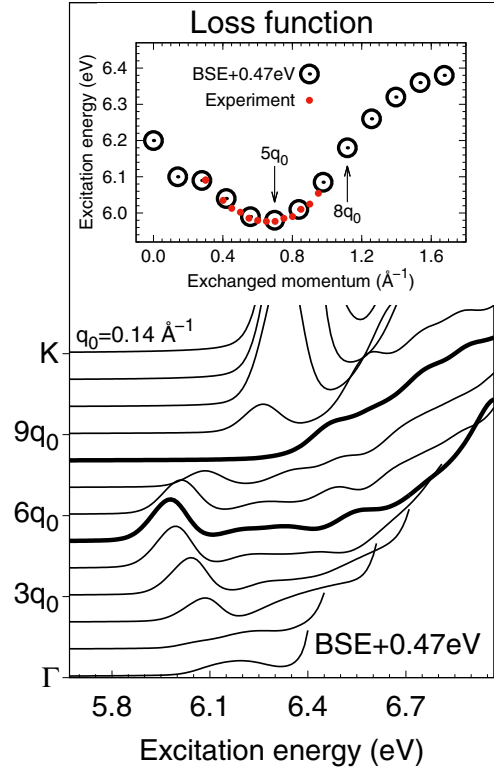FIG. 1. GW-BSE simulations of the loss function; thicker lines correspond to $q = 5q_0 = 0.7 \,\text{Å}^{-1}$ and $q = 8q_0 = 1.1 \,\text{Å}^{-1}$. (Inset) The peak dispersion compared against EELS measurements [7]. Simulated data have been blue-shifted by 0.47 eV.

appears clearly from Fig. 2, where we show that Im[ϵ] (dashed curve) and $L(\mathbf{q},\omega)$ (solid curve) at $\mathbf{q} = 5\mathbf{q}_0$ and $\mathbf{q} = 8\mathbf{q}_0$ present the same spectral features. Also, for either momentum, we mark the energy of the first six excitons, that is, $E_\lambda(\mathbf{q})$ for $\lambda \leqslant 6$, with colored circles whose size is proportional to $\log[I_\lambda(\mathbf{q})]$. The scale of the loss function in the two panels is the same, and similarly for the scale of Im[ϵ]. Additional information about the dispersion of the first six excitons can be found in Appendix B.

Furthermore, for $\mathbf{q} = 5\mathbf{q}_0$ we report the corresponding spectrum of Im[ϵ] without electron-hole interaction, i.e., taking into account only independent-particle (IP) transitions between GW levels (dot-dashed curve). This spectrum appears flat at 5.5 eV where the BSE calculation predicts a relatively sharp peak. This comparison confirms the hypothesis, already advanced in [7], that the peak has an excitonic nature.

In the following we will focus on the reason of the variations of intensity of the first peak, and in particular at momenta $\mathbf{q} = 5\mathbf{q}_0$ and $\mathbf{q} = 8\mathbf{q}_0$, where the intensity is at its highest and its lowest. Based on the observations detailed above, we will perform our analysis on Im[ϵ] instead of working with the more cumbersome loss function.

IV. EXCITON ANALYSIS AT q = 5q₀ ≈ 0.7 Å⁻¹

The excitonic peak at $\mathbf{q} = 5\mathbf{q}_0$ has a binding energy of 0.33 eV, that is, the energy difference with respect to the lowest IP transition with the same $\mathbf{q}$ (including G_0W_0 corrections).
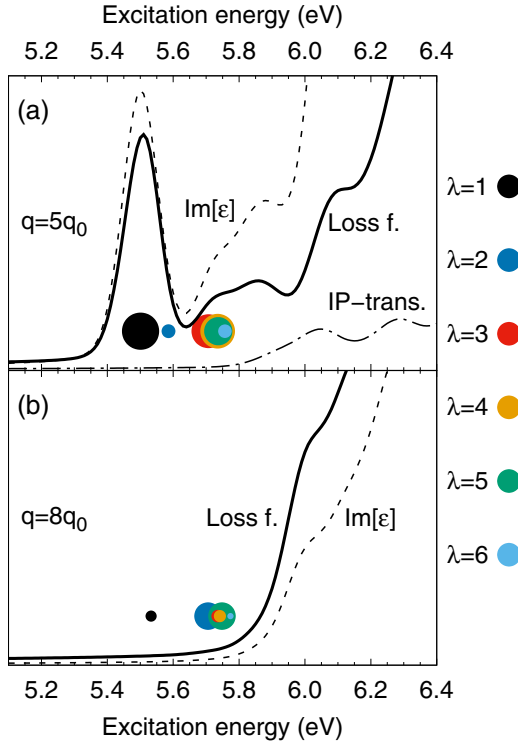
FIG. 2. (a) Simulated spectra of $L(\mathbf{q},\omega)$ (solid curve) and $\mathrm{Im}[\epsilon]$ with and without electron-hole interaction (dashed and dot-dashed curves), at $\mathbf{q} = 5\mathbf{q}_0 \approx 0.7\,\text{Å}^{-1}$. Circles mark the excitonic energies $E_\lambda(\mathbf{q})$ for $\lambda \leqslant 6$. (b) As in (a), but for the exchanged momentum $\mathbf{q} = 8\mathbf{q}_0 \approx 1.1\,\text{Å}^{-1}$. The calculation without electron-hole interaction is not reported.

In Fig. 3 the normalized cumulant weight defined in (4) is reported versus the energy E of the IP transitions. We observe that $\mathcal{J}_{\lambda=1}(5\mathbf{q}_0, E)$ is a monotonic function of E; it rises steeply up to $E \approx 6.8$ eV from where its derivative decreases
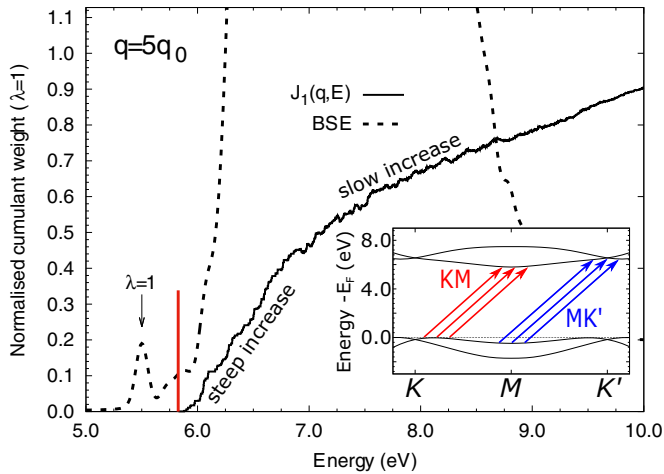

FIG. 3. Cumulant spectral weight (solid curve); GW-BSE spectrum (dashed curve) at $\mathbf{q} = 5\mathbf{q}_0$. A red vertical line marks the lowest IP transition. (Inset) The GW band structure along KMK' where the KM and MK' groups of IP transitions are sketched in red and blue, respectively.

mildly. Finally it reaches its asymptotic value of 1 at about $E \approx 12$ eV (not shown). What this tells us is that IP transitions sum up constructively at all energies, with most important contributions coming from transitions of energy $E < 6.8$ eV. Indeed these few transitions (0.4% of the total) account for almost the 42% of the spectral weight, as $\mathcal{J}_1(5\mathbf{q}_0, 6.8) = 0.42$ attests. Still, to get closer to the full spectral weight, one has to include higher-energy transitions. At $E = 9.5$ eV, 85% of the spectral weight is accounted for by still a relatively small number of transitions (less than 10% of the total).

We can now gain a deeper insight into the way IP transitions combine in forming the exciton by looking at the terms of the sum (3). Let us divide the latter group of transitions ($E \leqslant 9.5$ eV) in three categories: those transitions t for which both real and imaginary parts of the amplitude $M_t^\lambda(\mathbf{q})$ are negative, those for which both are positive and transitions where they have the opposite sign. The latter category turns out to be composed by transitions with amplitude $M_t^\lambda(\mathbf{q}) \approx 0$, so they do not contribute significantly to the exciton intensity and we can safely neglect them in the analysis. The other two groups enter the sum of Eq. (3) with different signs. Little more than one-third of the considered transitions falls into the first group, with negative amplitude $M_t^\lambda(\mathbf{q})$. They are mostly low-energy transitions. A cartography of these transitions is reported in Figs. 4(a) and 4(b), where $\log(|\sum_{v,c} M_{(v,\mathbf{k})\to(c,\mathbf{k}+\mathbf{q})}^{\lambda=1}(\mathbf{k})|)$ is reported as a function of the valence state $\mathbf{k}$ or conduction state $\mathbf{k} + \mathbf{q}$ for k points in the $\Gamma K M$ plane. On the other hand, slightly less than one-third of the transitions belong to the positive amplitude group, and they have higher energy but in general lower intensity. Their maps are reported in Figs. 4(c) and 4(d).

The analysis suggests the following interpretation. Two groups of transitions participate in the formation of the bright exciton ($\lambda = 1$), observed in Ref. [7]. One group (let us call it the KM group) is composed mostly of low-energy transitions going from points close to K to points close to M (and similarly $H \to L$ in the AHL plane, reported in Appendix D). The lowest-energy transitions of this group have also the larger amplitude (in absolute value) $|M_t^\lambda(\mathbf{q})|$, and they sum constructively in the steep part of the cumulant ($E < 6.8$ eV). At higher energy, a second group of IP transitions (call it the MK' group), from points in the vicinity of M to points in the vicinity of K' (and $L \to H'$) enter the sum with opposite amplitude, hence canceling partially the contribution of the KM group. This explains why the derivative of the cumulant decreases from 6.8 eV on, but it is still positive because of the larger number and higher absolute amplitude of the dominating KM group.

The origin of the peak being established, we can now draw the connection with the single-particle band structure. In the inset of Fig. 3 we report the GW band structure along the relevant path KMK', in good agreement with previous calculations [5,6,9,16] and experiments [17]. The KM and the MK' groups of transitions have been sketched with colored arrows, respectively, red and blue. At this $\mathbf{q}$, the KM group of transitions is basically the indirect transition between the top valence and the bottom of conduction. The fact that the top valence is close to, but does not coincide with K, is consistent with the fact that the lowest excitation is found at $\mathbf{q} < 8.4\,\text{Å}^{-1}$. The strength of the peak is explained by the
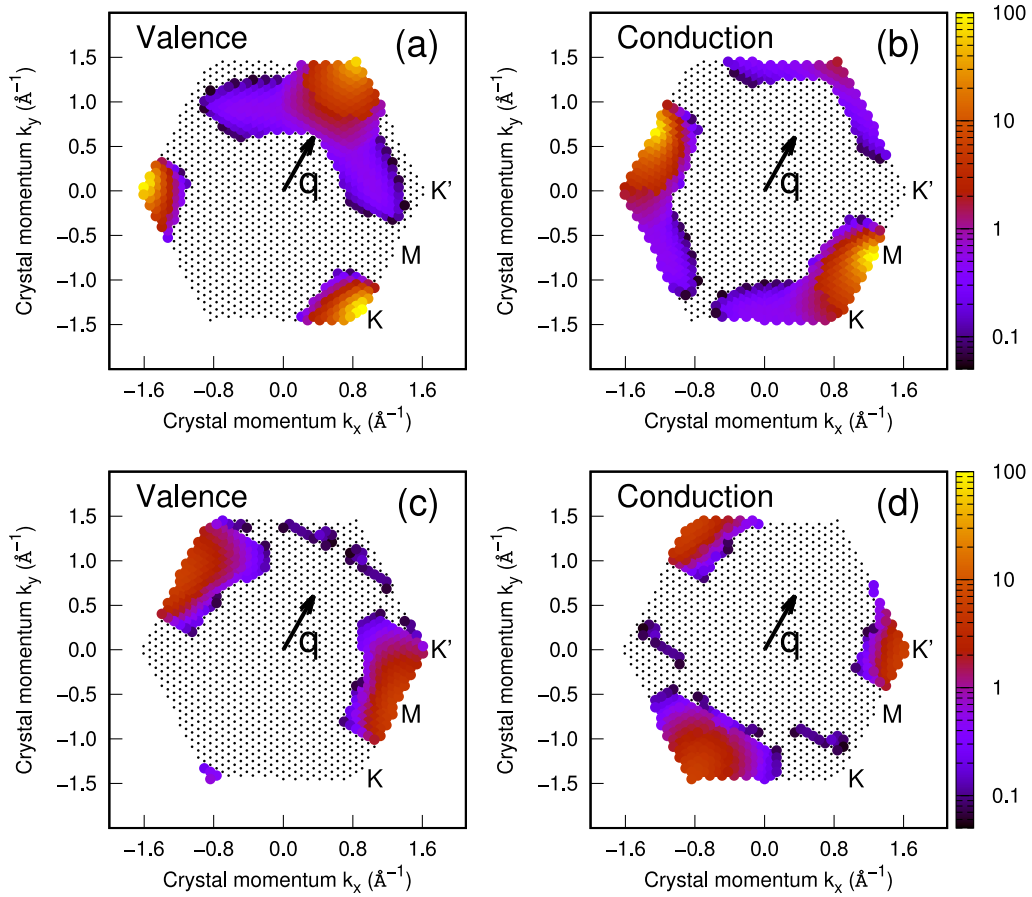
FIG. 4. (Top) Transition cartographies of the KM group at $\lambda = 1$ and $\mathbf{q} = 5\mathbf{q}_0$ plotted for k points in the $\Gamma K M$ plane for valence (a) and conduction states (b). (Bottom) The same for the MK' group.

fact that the KM transitions take place between regions of the band structure where bands are particularly flat (van-Hove singularities). Also, the convex curvature of the band structure explains why the MK' transitions start contributing at higher energy and have lower amplitude.

V. EXCITON ANALYSIS AT $q = 8q_0 \approx 1.1\,\text{Å}^{-1}$

Let us switch now to $\mathbf{q} = 8\mathbf{q}_0$. At this momentum, the spectral weight is dramatically reduced and it is moved from $\lambda = 1$ to a group of higher-energy excitons among which $\lambda = 2$ and $\lambda = 5$ have the highest (although still very weak) intensity. In the $\lambda = 2$ case, the normalized cumulant weight, reported in Fig. 5 does not grow monotonically, instead first it explodes for $E \leqslant 6.8$ eV, where it attains the value of ~ 50, then it attains its maximum between 7 and 7.8 eV and then decreases to reach the asymptotic limit at about 12 eV. We can perform the same analysis as before for IP transitions of energy $E \leqslant 9.5$ eV. The cartographies of the IP transitions are reported in Figs. 6(a) and 6(b) for the KM group, and Figs. 6(c) and 6(d) for the MK' group. At variance with the case before the amplitudes of KM and MK' transitions are closer.

These results can be rationalized as follows. Most of the IP transitions entering in $I_{\lambda=2}(\mathbf{q})$ up to 6.8 eV are of the KM group and they sum constructively. But at higher energy, the MK' transitions, which contribute with the opposite sign, start having comparable importance. This induces a halt in

the increasing trend ($6.8 < E < 7.8$ eV) and eventually they dominate bending down the cumulant back to its asymptotic limit. The result is that the two groups of transitions almost cancel each other, leading to a very weak intensity.
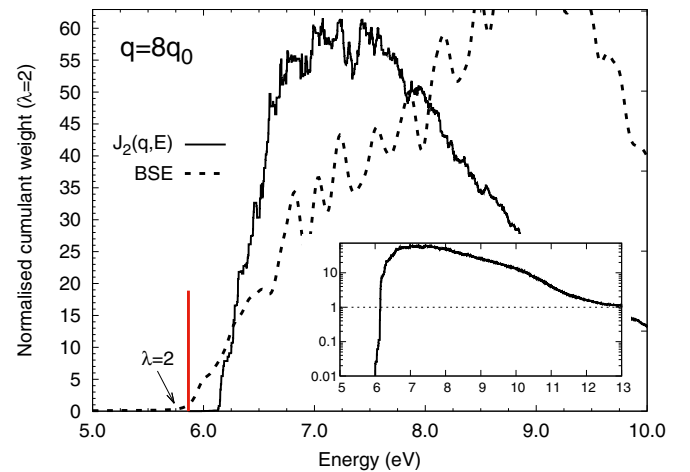

FIG. 5. Cumulant spectral weight (solid curve); GW-BSE spectrum (dashed curve). A red vertical line marks the energy of the lowest IP transition. (Inset) The cumulant spectral weight up to $E < 13$ eV in the logarithmic scale.
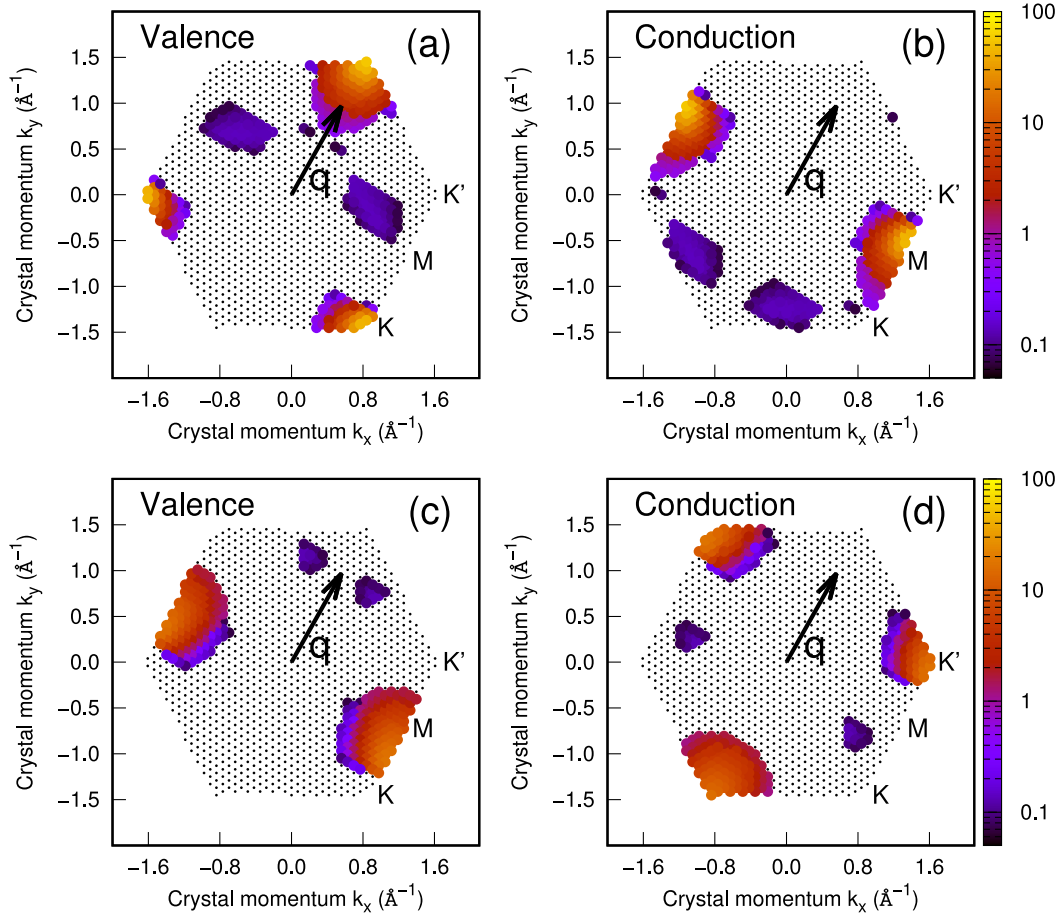
FIG. 6. (Top) Transition cartographies of the KM group at $\lambda = 2$ and $\mathbf{q} = 8\mathbf{q}_0$ plotted for k points in the ΓKM plane for valence (a) and conduction states (b). (Bottom) The same for the MK' group.

It is worth recalling here that the $\lambda = 2$ exciton is almost degenerate with another exciton of non-negligible intensity ($\lambda = 5$). Not surprisingly, carrying out a similar analysis on the latter leads to basically the same results (see Appendix C).
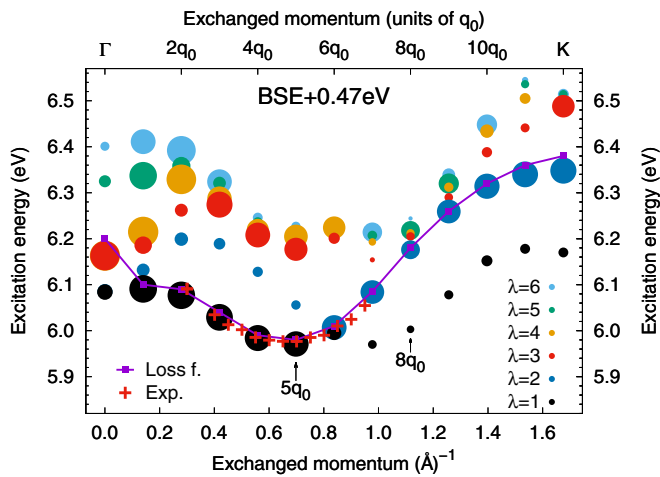

FIG. 7. Dispersion of the excitonic energies $E_\lambda(\mathbf{q})$ for $\lambda \leqslant 6$. The size of the circles is proportional to the logarithm of the peak intensity. A purple line connects the lowest peaks of the loss function $L(\mathbf{q}, \omega)$. Red crosses are the peak of the experimental loss function extracted from [7]. All calculated points have been blue-shifted by 0.47 eV.
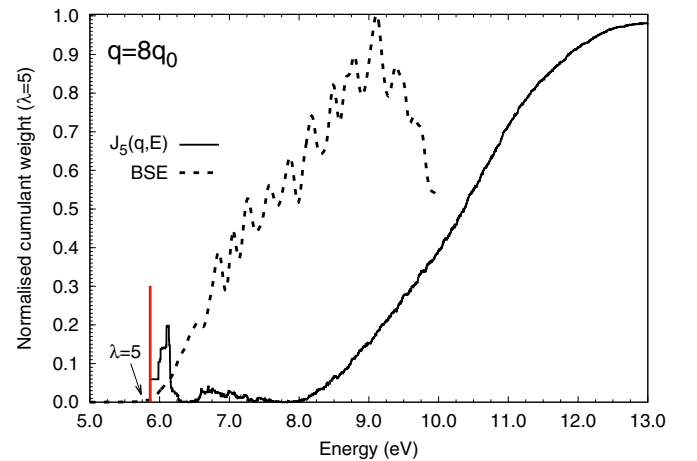

FIG. 8. Cumulant spectral weight (solid curve) of the $\lambda = 5$ exciton and the corresponding GW-BSE spectrum (dashed curve) at $\mathbf{q} = 8\mathbf{q}_0$. A red vertical line marks the energy of the lowest IP transition.
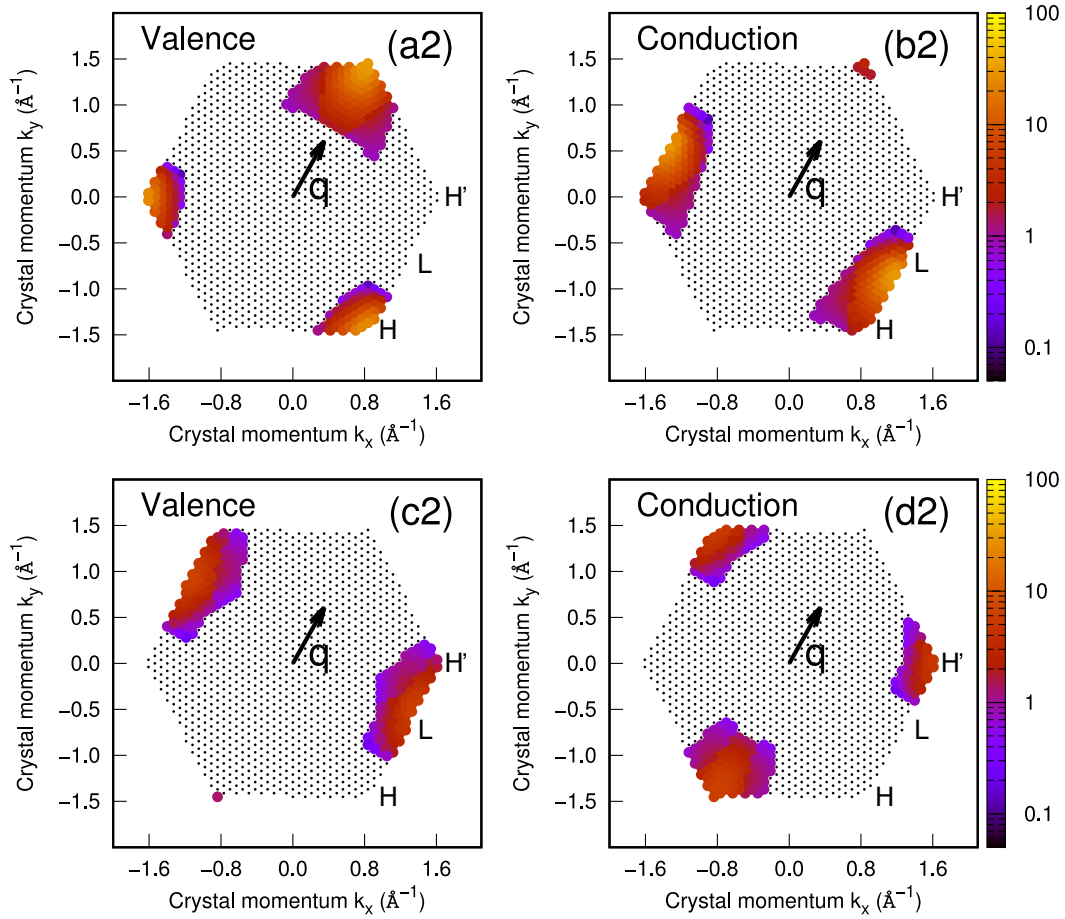
FIG. 9. (Top) Transition cartographies of the KM group at $\lambda = 1$ and $\mathbf{q} = 5\mathbf{q}_0$ plotted for k points in the AHL plane for valence (a2) and conduction states (b2). (Bottom) The same for the MK' group.

VI. CONCLUSIONS

We computed the loss function of bulk h–BN solving the *ab initio* GW-Bethe-Salpeter equation at finite $\mathbf{q}$ along the ΓK direction, which is relevant for spectroscopic studies. We observe an excitonic peak dispersing of about 0.45 eV, displaying a strong intensity at $\mathbf{q} \approx 0.7 \,\mathring{A}^{-1}$, where the excitation energy is the lowest, and almost disappearing at $\mathbf{q} \approx 1.1 \,\mathring{A}^{-1}$. These findings are in very good agreement with recent electron energy loss experiments [7].

The associated dielectric function displays similar characteristics. We show that the peak intensity is determined by the interference of two groups of transitions contributing to the peak formation with opposite signs. Our investigation allow us to unveil a nontrivial connection between the exciton dispersion, its intensity, and the electronic structure in the vicinity of $K(H)$ and $K'(H')$ points in bulk h–BN, eventually suggesting ways to control excitonic properties by changing the electronic structure in the vicinity of the K and K' valleys. It is worth stressing that with the help of the methodology we devised, it is possible to use spectroscopic methods to probe electronic excitations at the two valleys at the same time. This is of paramount importance, for instance, in the valleytronics of layered systems [18].

Furthermore, the methodology presented in this work is of general applicability and could be extended to studies of excitonic properties in any system. The splitting of relevant IP transitions into appropriately defined groups can simplify the interpretation of the excitonic properties, help the analysis, and possibly disclose some nontrivial mechanism. We believe that the strategy adopted here can be employed successfully also to other cases in bulk as well as in two-dimensional (2D) materials. This helps the interpretation of measured data (as the case of our application to h–BN) but most importantly it can suggest where and how to change the electronic structure whenever a control on the excitonic intensity is required.

APPENDICES

APPENDIX A: COMPUTATIONAL DETAILS

The simulated h–BN has lattice parameters $a = 2.5 \,\mathring{A}$ and $c/a = 2.6$ [19]. The Kohn-Sham system and the GW
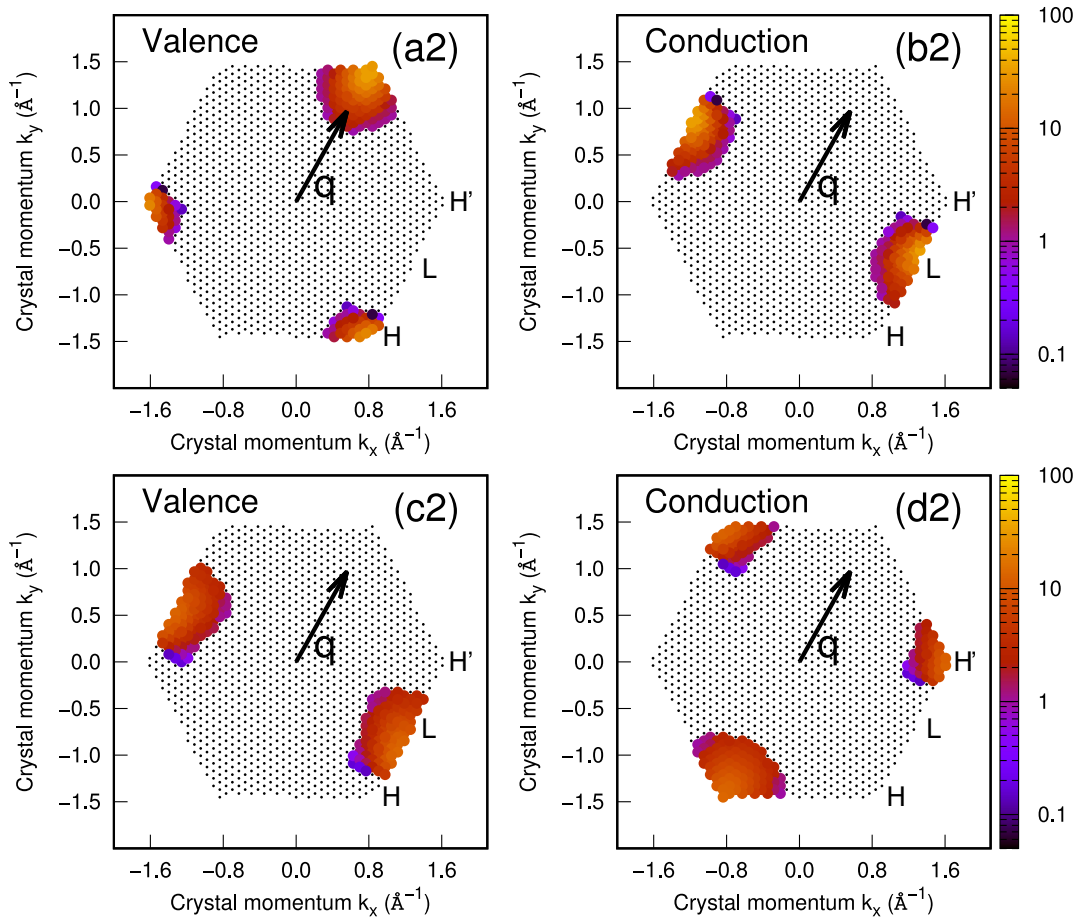
FIG. 10. (Top) Transition cartographies of the KM group at $\lambda = 2$ and $\mathbf{q} = 8\mathbf{q}_0$ plotted for k points in the AHL plane for valence (a2) and conduction states (b2). (Bottom) The same for the MK' group.

corrections have been computed with the ABINIT simulation package (a plane-wave code [20]). Norm-conserving Troullier-Martins pseudopotentials have been used for both atomic species. DFT energies and wave functions have been obtained within the local density approximation (LDA) to the exchange-correlation potential, using a plane-wave cutoff energy of 30 Ha and sampling the Brillouin zone with a $8 \times 8 \times 4$ Γ-centred k-point grid. The GW quasiparticle corrections have been obtained within the perturbative GW approach. They have been computed on all points of a $6 \times 6 \times 4$ Γ-centered grid; a cutoff energy of 30 Ha defines the matrix dimension and the basis of wave function for the exchange part of the self-energy. The correlation part has been computed including 600 bands and applying the same wave function basis as before. To model the dielectric function, the contour deformation method has been used, computing the dielectric function up to 60 eV, summing over 600 bands and with a matrix dimension of 6.8 Ha. The quasiparticle corrections have been subsequently interpolated on a denser $36 \times 36 \times 4$ k-point grid where the BSE calculation has been carried out.

The macroscopic dielectric function $\epsilon(\mathbf{q}, \omega)$ has been calculated at the GW-BSE level in the Tamm-Dancoff approximation using the code EXC [21]. We included six valence bands and three conduction bands; 360 eV is the cutoff energy for both the matrix dimension and the wave-function basis. The static dielectric matrix entering in the BSE kernel has been

computed within the random phase approximation with local fields, including 350 bands and with a cutoff energy of 120 eV and 200 eV for the matrix dimension and the wave-function basis, respectively. With these parameters, the energy of the first peaks of $\epsilon(\mathbf{q}, \omega)$ are converged within 0.01 eV and their intensity are converged within 5%.

All reported spectra have been convoluted with a Gaussian of $\sigma = 0.05$ eV in order to reduce the noise due to the discrete k-point sampling and to simulate the experimental broadening.

APPENDIX B: DISPERSION OF THE FIRST SIX EXCITONS

In Fig. 7 we report the dispersion of the first six excitons along the line ΓK with colored circles whose size is proportional to $\log[I_\lambda(\mathbf{q})]$, so larger circles correspond to bright excitations. The points have been obtained within the GW-BSE framework and shifted by 0.47 eV to higher energies.

As expected [9,16,22], at $\mathbf{q} = \Gamma$ the first two excitons are degenerate and basically dark, whereas all the peak intensity is concentrated on the degenerate excitons with $\lambda = 3$ and 4 (the two are superimposed in the plot, so that only $\lambda = 3$ is visible). As soon as one moves away from Γ, the degeneracy is lifted [22] and the first bright peak coincides with the lowest energy exciton ($\lambda = 1$). This is valid up to $\mathbf{q} \approx 6\mathbf{q}_0$ (halfway in the ΓK line) where the peak intensity is moved to $\lambda = 2$ as a consequence of a band crossing. The intensity of

the excitations is successively reduced at $8\mathbf{q}_0$ and $9\mathbf{q}_0$ where several excitons are concentrated in a narrow energy range. Finally, as $\mathbf{q}$ approaches K, the exciton $\lambda = 2$ steps up again concentrating most of the intensity.

We also report on the same figure the dispersion of the loss function as measured [7] (red crosses) and computed in this work (purple squared curve). One can see that the position of the peak of $L(\mathbf{q},\omega)$ follows closely the dispersion of the first bright excitation of Im[ϵ] (lowest energy larger circles).

APPENDIX C: ANALYSIS OF THE $\lambda = 5$ EXCITON AT q = 8q$_0$

At $\mathbf{q} = 8\mathbf{q}_0$, the intensity of the peak is very low. This low intensity is basically shared by two excitons, $\lambda = 2$ (analyzed in the main text) and $\lambda = 5$ with an energy around 50 meV higher. The analysis with the cumulant weight, reported in Fig. 8, has a surprising shape. After a first increase around 6 eV, the cumulant decreases abruptly and vanishes at 6.5 eV.

Then it oscillates around the value 0 until one starts including IP transitions of energy $E \geqslant 8.0$ eV. Remembering that cumulant weight is defined as a modulus squared, one realizes immediately that what is observed is again a phenomenon of interference (as in the $\lambda = 2$ case), but the dominating group changes during the analysis. At the very beginning ($E \leqslant$ 6.1 eV) the KM group constructs the peak, but immediately after the MK' transitions cancel this contribution and lead the cumulant weight back to 0. From this point, the two contributions mutually cancel and it is only at $E > 8$ eV that the MK' group prevails and the cumulant starts growing monotonically to its asymptotic limit.

APPENDIX D: ANALYSIS AT q = 5q$_0$ AND q = 8q$_0$ ON THE AHL PLANE

In the main text, Figs. 4 and 6 have been obtained taking $\mathbf{k}$ points in the ΓKM plane. In Figs. 9 and 10 we report the cartographies of the KM and MK' groups in the AHL plane of the Brillouin zone.

[1] K. Watanabe, T. Taniguchi, and H. Kanda, Nat. Mater. **3**, 404 (2004).

[2] P. Jaffrennou, J. Barjon, J.-S. Lauret, B. Attal-Trétout, F. Ducastelle, and A. Loiseau, J. Appl. Phys. **102**, 116102 (2007).

[3] G. Cassabois, P. Valvin, and B. Gil, Nat. Photonics **10**, 262 (2016).

[4] L. Schué, B. Berini, A. C. Betz, B. Plaçais, F. Ducastelle, J. Barjon, and A. Loiseau, Nanoscale **8**, 6986 (2016).

[5] S. Galambosi, L. Wirtz, J. A. Soininen, J. Serrano, A. Marini, K. Watanabe, T. Taniguchi, S. Huotari, A. Rubio, and K. Hämäläinen, Phys. Rev. B **83**, 081413(R) (2011).

[6] G. Fugallo, M. Aramini, J. Koskelo, K. Watanabe, T. Taniguchi, M. Hakala, S. Huotari, M. Gatti, and F. Sottile, Phys. Rev. B **92**, 165122 (2015).

[7] R. Schuster, C. Habenicht, M. Ahmad, M. Knupfer, and B. Büchner, Phys. Rev. B **97**, 041201(R) (2018).

[8] F. Fossard, L. Sponza, L. Schué, C. Attaccalite, F. Ducastelle, J. Barjon, and A. Loiseau, Phys. Rev. B **96**, 115304 (2017).

[9] B. Arnaud, S. Lebègue, P. Rabiller, and M. Alouani, Phys. Rev. Lett. **96**, 026402, (2006); L. Wirtz, A. Marini, M. Grüning, C. Attaccalite, G. Kresse, and A. Rubio, *ibid.* **100**, 189701 (2008).

[10] G. Strinati, La Rivista del Nuovo Cimento **11**, 1 (1988).

[11] M. Gatti and F. Sottile, Phys. Rev. B **88**, 155113 (2013).

[12] P. L. Cudazzo, F. Sottile, A. Rubio, and M. Gatti, J. Phys.: Condens. Matter **27**, 113204 (2015).

[13] G. Onida, L. Reining, and A. Rubio, Rev. Mod. Phys. **74**, 601 (2002).

[14] P. K. Gogoi, L. Sponza, D. Schmidt, T. C. Asmara, C. Diao, J. C. W. Lim, S. M. Poh, S.-I. Kimura, P. E. Trevisanutto, V. Olevano, and A. Rusydi, Phys. Rev. B **92**, 035119 (2015).

[15] L. Wirtz, A. Marini, and A. Rubio, Phys. Rev. Lett. **96**, 126104 (2006).

[16] T. Galvani, F. Paleari, H. P. C. Miranda, A. Molina-Sánchez, L. Wirtz, S. Latil, H. Amara, and F. Ducastelle, Phys. Rev. B **94**, 125303 (2016).

[17] H. Henck, D. Pierucci, G. Fugallo, J. Avila, G. Cassabois, Y. J. Dappe, M. G. Silly, C. Chen, B. Gil, M. Gatti, F. Sottile, F. Sirotti, M. C. Asensio, and A. Ouerghi, Phys. Rev. B **95**, 085410 (2017).

[18] H. Yuan, Z. Liu, G. Xu, B. Zhou, S. Wu, D. Dumcenco, K. Yan, Y. Zhang, S.-K. Mo, P. Dudin, V. Kandyba, M. Yablonskikh, A. Barinov, Z. Shen, S. Zhang, Y. Huang, X. Xu, Z. Hussain, H. Y. Hwang, and Y. Cui, and Y. Chen, Nano Lett. **16**, 4738 (2016).

[19] V. L. Solozhenko, G. Will, and F. Elf, Solid State Comm. **96**, 1 (1995).

[20] http://www.abinit.org/.

[21] http://etsf.polytechnique.fr/exc/.

[22] J. Koskelo, G. Fugallo, M. Hakala, M. Gatti, F. Sottile, and P. Cudazzo, Phys. Rev. B **95**, 035125 (2017).